4-15-2014

Development of a Silicon PIN Diode X-Ray Detector

Joshua Abramovitch
Southern Methodist University, jabramovit@gmail.com

Development of a Silicon PIN Diode X-Ray Detector

Primary Author: Joshua Abramovitch
Mentor: Dr. Andy Liu

I. Introduction

Many methods used to calculate x-ray flux are incapable of accounting for the high x-ray flux generated by modern x-ray machines. The most common method utilized today for monitoring x-ray dose rate in real time, by ionizing gas chambers, is usable for modern devices but is technically complex. The construction of a gas chamber is not a simple task, and its large size necessitates gas tubing, high voltages, signal cables, and other specialized parts and services to operate. The ionization approach is impractical for certain applications, such as when radiation dose must be measured in confined spaces. Advances in the technology of silicon PIN diodes in the datacom and telecom industries allow for the development of an inexpensive and compact solid-state ionizing sensor to calculate x-ray flux. As x-ray photons flux through the diodes, the photoelectric effect produces a photocurrent (1). The x-ray flux can be determined from this current, and once the former is known the radiation dose can be calculated from it.

II. Characterization of β, γ, and μ Events

To establish a theoretical foundation, particle impact events on the silicon PIN photodiode were observed and the charge and energy deposited were estimated. Most of the experiments conducted at this stage utilized commercially-available devices, a Cremat CR-110 charge-sensitive preamplifier (CSP) and a Cremat CR-200 Gaussian shaping amplifier (GSA). The gain of the GSA was set to 10, and the gain of the CSP was 1.4 V/pC. Although expensive and requiring two stages, the commercial devices produced clean output and allowed for the observation of said events via digital oscilloscope. Initially, the objective was to compare the signals produced by alpha (α), beta (β), and gamma (γ) button sources. Figures 1 and 2 below show the pulse produced by β particle and γ photon events; no α events were observed because α particles could not penetrate the plastic housing of the diodes. The β pulses were on average 750 mV in amplitude while the γ pulses were smaller, 300 mV in amplitude on average. Even though γ photons possess high energy, they are significantly more penetrating than β particles and as such did not deposit all of their energy onto the diode during an event.

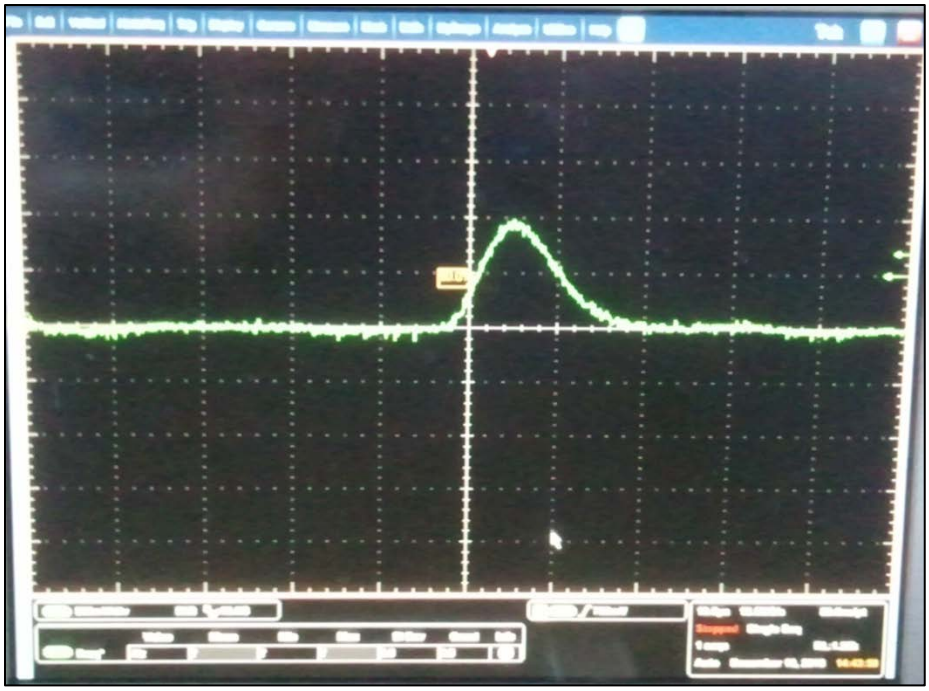

Figure 1 – Typical β Event (500 mV/division)

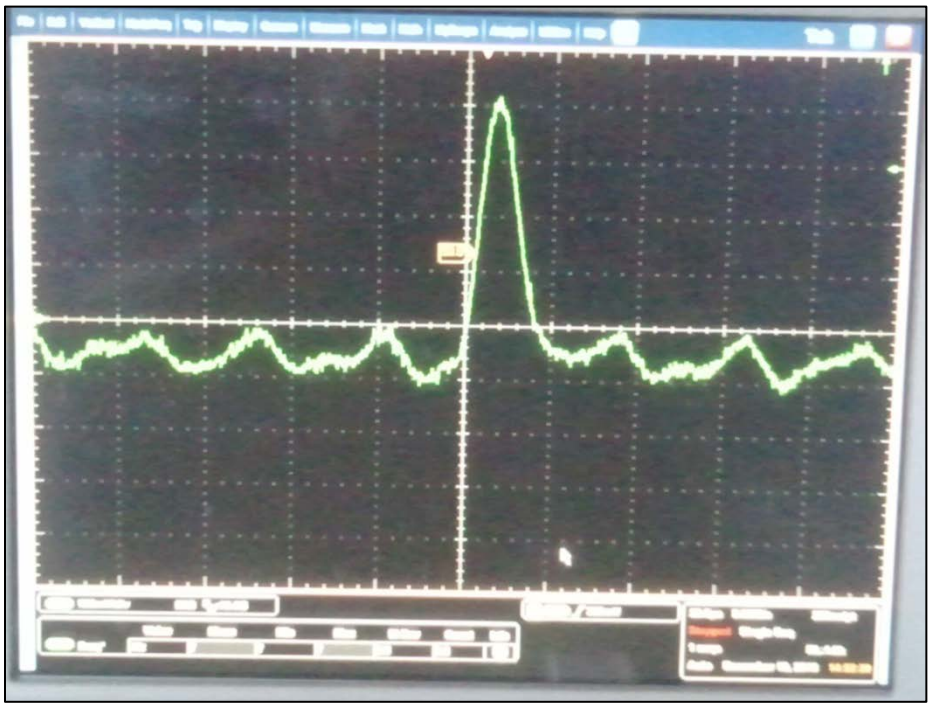

Figure 2 – Typical γ Event (75 mV/division)

A cosmic muon (μ) detection experiment was conducted with 4 silicon PIN diodes (Vishay VBPW34FAS), each of sensitive area 7.5 mm^2 for a total sensitive area of 30 mm^2, or 0.3 cm^2. Also used were the Cremat CSP, the Cremat GSA, and an Agilent frequency counter. Over a period of ~18.5 hours, a frequency of ~1.6 mHz was recorded; this corresponds to 107 events over the entire period, or on average approximately 1 event every 10 minutes. Such an event rate

is reasonable, if somewhat low; a more typical cosmic muon rate is 0.8 events per cm^2 per minute at sea level (2). Accounting for the total sensitive area of the diodes, this rate equates to approximately 1 event every 4 minutes.

The next day, the output of 15 additional cosmic ray events was captured and analyzed. A typical cosmic μ pulse is shown in Figure 3. The average amplitude was 1 V, in contrast with the 750 mV average β amplitude and the 300 mV average γ amplitude.

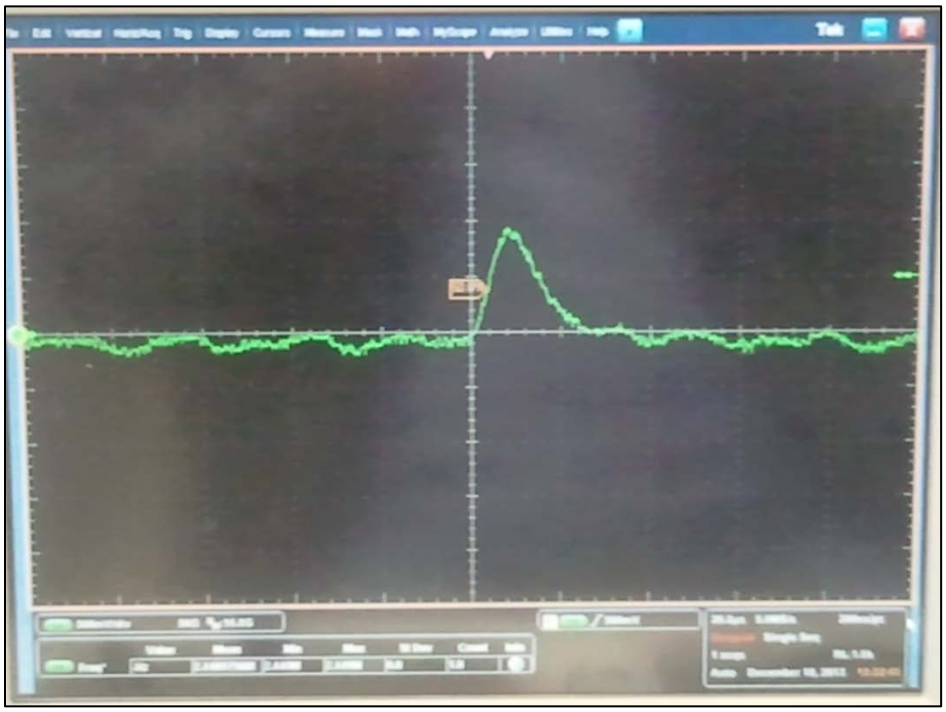

Figure 3 – Typical μ Event

A series of the calculations were then performed to estimate the charge and energy deposited for each type of event. Each voltage was then divided by the GSA gain to determine the output voltage of the CSP. The GSA gain was determined by dividing the peak-to-peak output voltage by the peak-to-peak input voltage of a sine wave function; 1.16 $V_{pp,out}$ divided by 100 $mV_{pp,in}$ resulted in an estimated GSA gain of 11.6. The charge Q_{dep} deposited onto the photodiode for an event was calculated by dividing $V_{CSP,out}$ by the CSP gain of 1.4 V/pc. Finally, the energy deposited onto the photodiode was determined by multiplying Q_{dep} by the band gap of pure silicon (1.1 eV) and dividing by the charge of an electron ($1.602*10^{-19}$ C). Table 1 below lists the charge and energy deposited for each type of event.

Table 1 – Charge and energy deposited

Event	Q_{dep} (fC)	E_{dep} (MeV)
Cosmic muon (μ)	61.6	0.423
Beta particle (β)	46.2	0.317
Gamma photon (γ)	18.5	0.127

In addition, the feedback capacitance of the CSP was calculated to be 0.714 pF.

III. AC Circuit Design and Prototypes

The first type of circuit developed was AC-coupled, intended to produce pulses for use as a pulse counter. The design is based on one submitted to Radiation-Watch.org, a non-profit project initiated after the Fukushima Daiichi nuclear disaster, for a compact radiation counter that can be used with an iPhone (3). A schematic of the circuit used in the Radiation-Watch.org Pocket Geiger Type 1 is shown in Figure 4.

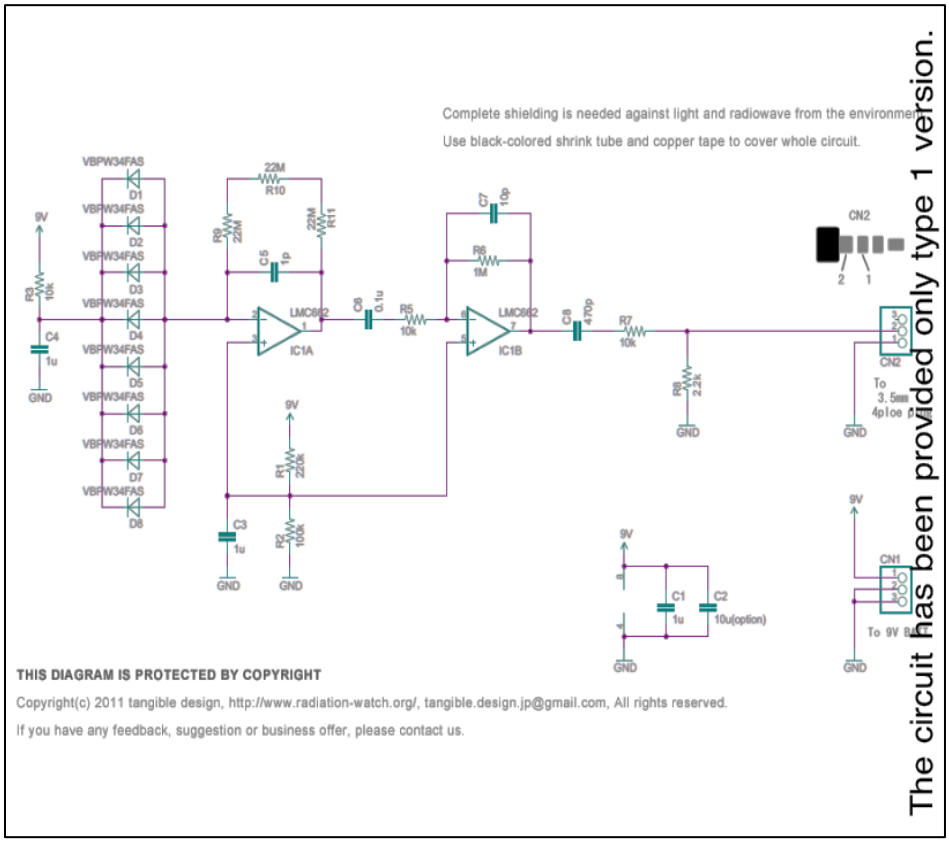

Figure 4 – Schematic of Type 1 Circuit (3)

Up to eight PIN photodiodes are placed in reverse bias, with the positive end connected to the first amplification stage. When a gamma ray strikes one of the photodiodes, a photocurrent is produced. The current then goes through two stages of transimpedance amplification to produce an output voltage. The capacitors immediately after each op-amp serve to eliminate DC offset. As a result, the circuit only registers pulses when a photon interacts with a photodiode. Additional resistors and capacitors are used to filter the output and reduce noise.

Four prototypes of the AC-coupled circuit, shown in Figures 5-8, were made following the Type 1 schematic. The AC-coupled circuits utilized off-the-shelf electronic components – resistors, capacitors, op-amps (Texas Instruments LMC662CN), and PIN diodes (Vishay VBPW34FAS) – and were designed to be powered by a 9V battery. Each successive prototype was made more compact, with components arranged more closely together and with less exposed wiring, to reduce noise in the output.

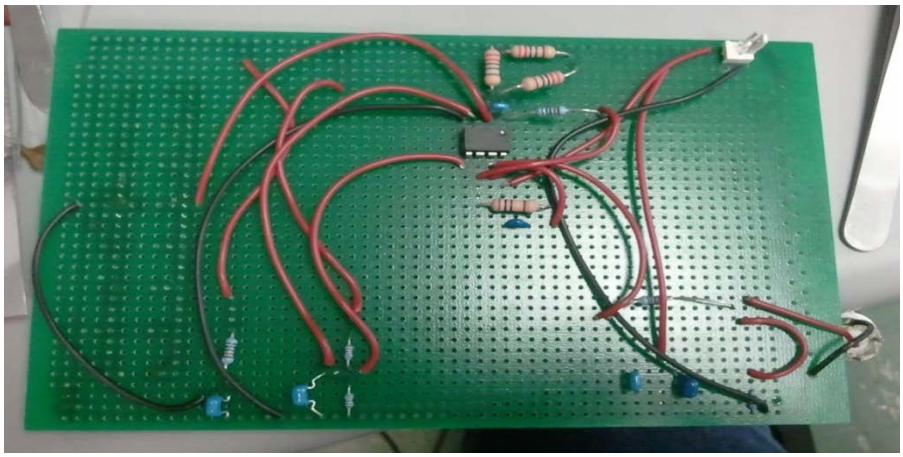

Figure 5 – AC Prototype 1

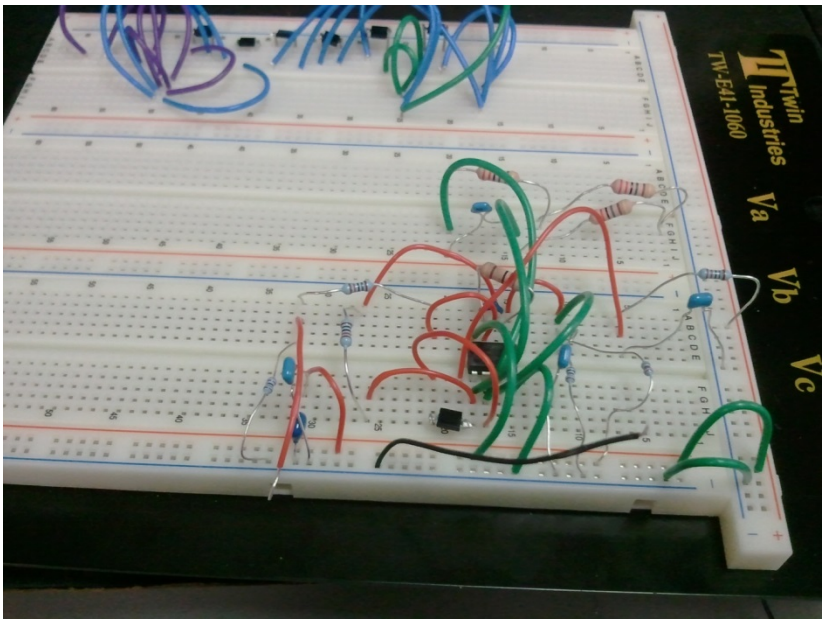

Figure 6 – AC Prototype 2

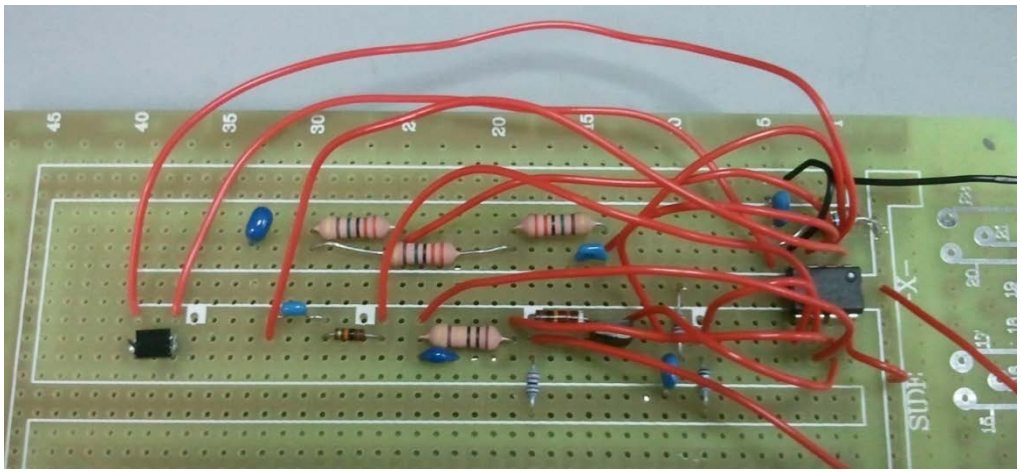

Figure 7 – AC Prototype 3

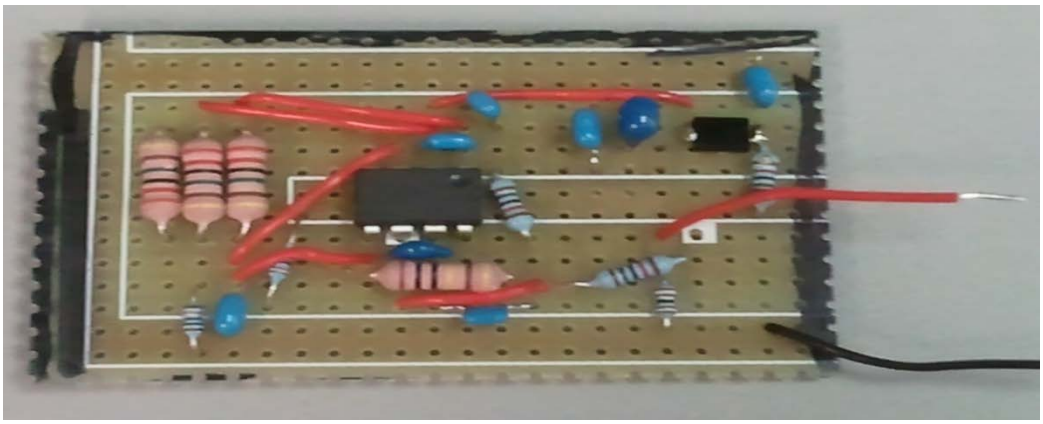

Figure 8 – AC Prototype 4

AC Prototype 4 was placed in a black, light-tight plastic, connected to a 9V battery, and tested in BNL's gamma irradiation chamber. In this dark, quiet environment, the output registered pulses for incident gamma rays from a button source at a low dose rate. As shown in Figure 9, the pulses were on the order of 10 mV. Placing the circuit close to the chamber's ^{60}Co gamma source for a higher dose rate resulted in many overlapping pulses of average amplitude 40 mV, as depicted in Figure 10.

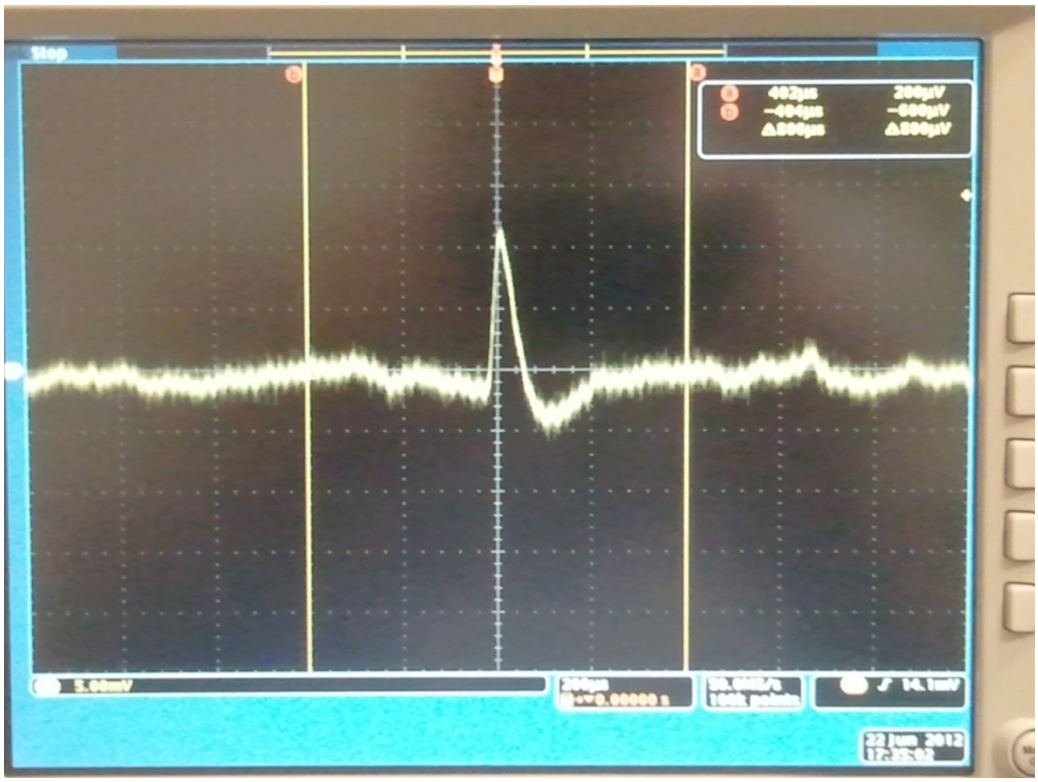

Figure 9 – AC Prototype 4 Output for a Low Dose Rate (Button Source)

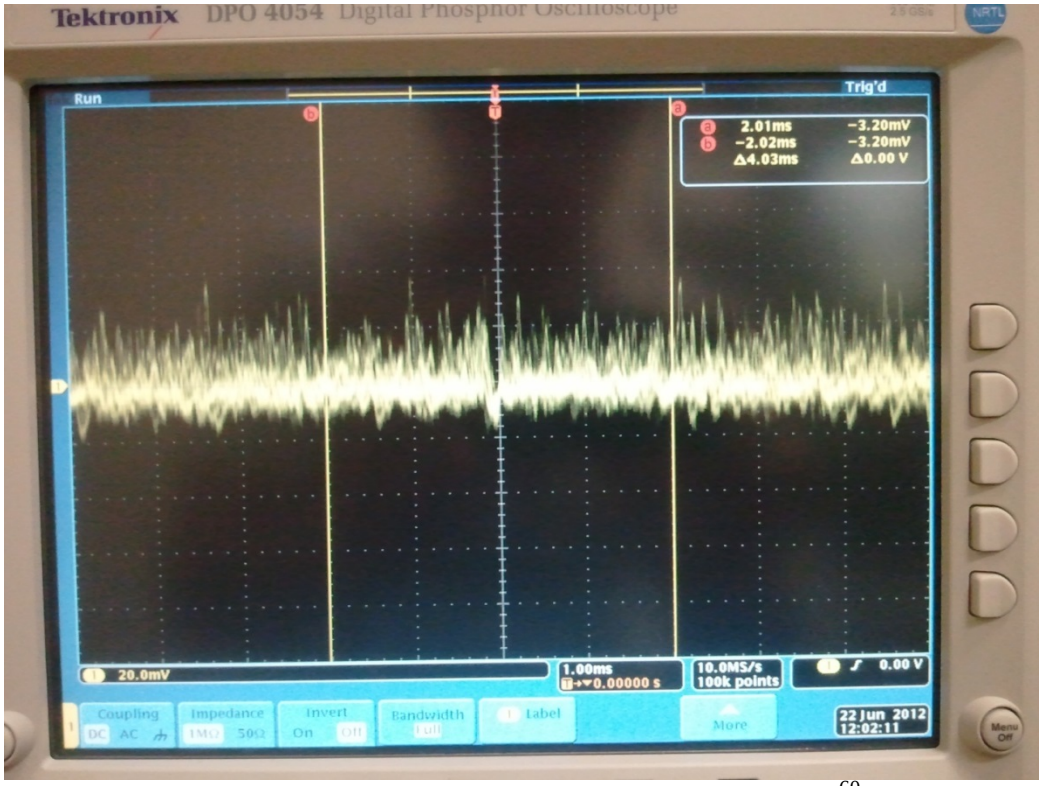

Figure 10 – Circuit 4 Output for a Higher Dose Rate (Close to ^{60}Co Source)

Attempts were then made to increase the circuit's gain and improve its ability to filter noise. However, these efforts were unsuccessful. Upon further examination of the circuit's design, it was determined that the second amplification stage acts as a band-pass filter and that the circuit as a whole is a series of intricately connected filters; changing even one component disrupted the balance and rendered the circuit useless. Acting on the band-pass idea, however, the circuit's output was routed through a sound card and recorded with Audacity, a free downloadable audio manipulation program. After much amplification, the resulting waveforms looked exactly like the outputs displayed on the oscilloscope. Incident gamma photons registered as clicks, much like those of a Geiger counter, while other background noise resulted in much more discordant and jarring sounds. Attempts to filter the output, amplify the clicks, and reduce other noise did not meet any success, so this side effort was abandoned.

After the tests at BNL were completed, printed circuit boards (PCBs) were designed with DesignSpark PCB, a free downloadable circuit design program. PCBs allow for the use of surface-mount components and for the elimination of any external wiring, resulting in a cleaner and less noisy circuit. Figure 11 shows a schematic of the AC circuit PCB, and Figure 12 depicts a 3D rendering of the PCB. All of the resistors and capacitors were surface-mount, but the op-amp was through-hole because a surface-mount equivalent was not available. The PIN diodes were not mounted to the PCB, but rather intended to be mounted to a probe and linked to the PCB at the IN connection. The AC PCB is compact, measuring 1.5 inches on each side. The four circles at the corners can be drilled to facilitate mounting in a light-tight container.

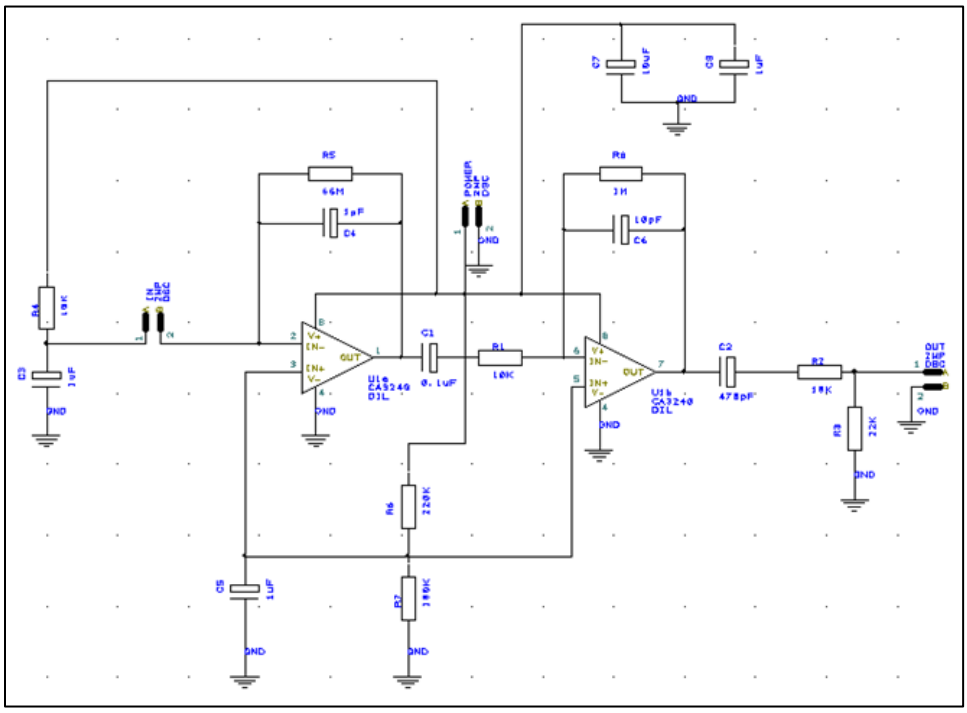

Figure 11 – AC PCB Schematic

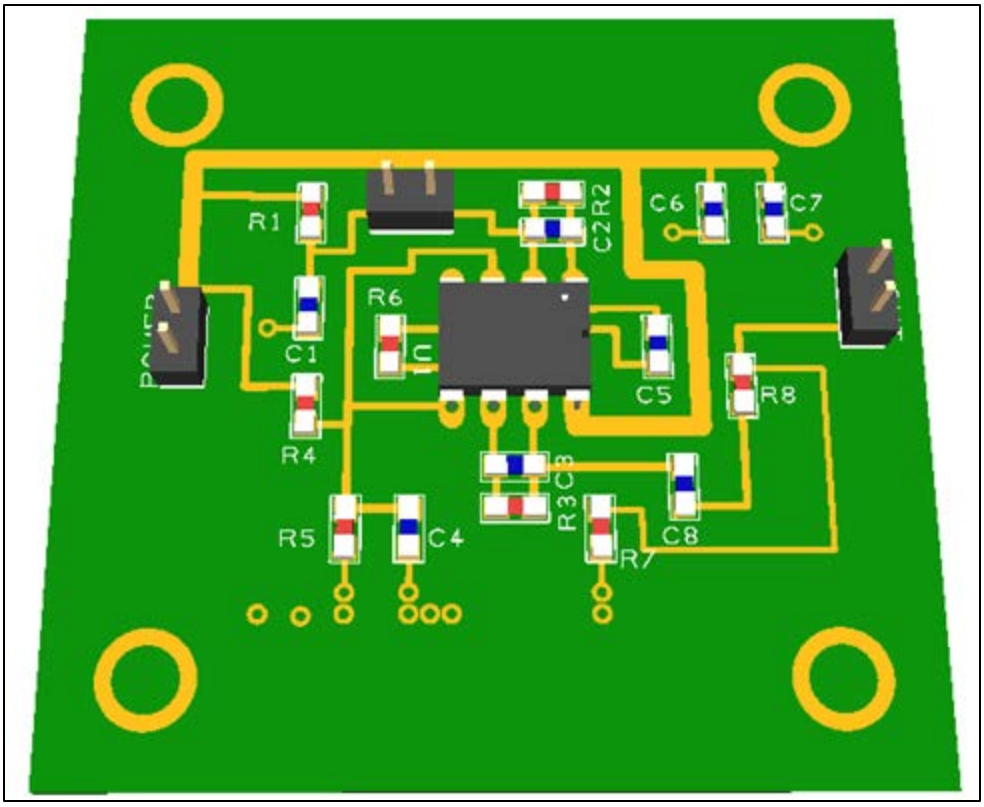

Figure 12 – AC PCB Rendering

IV. DC Circuit Design and Prototypes

The design of the AC circuit was altered to produce a DC-coupled circuit. Three PIN diodes were placed in forward bias, with the positive ends connected to ground and the negative ends connected to the negative input of the first op-amp. The positive input of the first op-amp was connected to ground with a 910k resistor to reduce bias current and also to reference the output to ground. The second amplification stage was changed to a simple non-inverting amplifier. A 10 pF and a 10 μF capacitor, placed in parallel with the second op-amp's positive input and with the circuit's output (respectively), served to filter noise. Figure 13 depicts and hand-drawn schematic of the DC circuit's design.

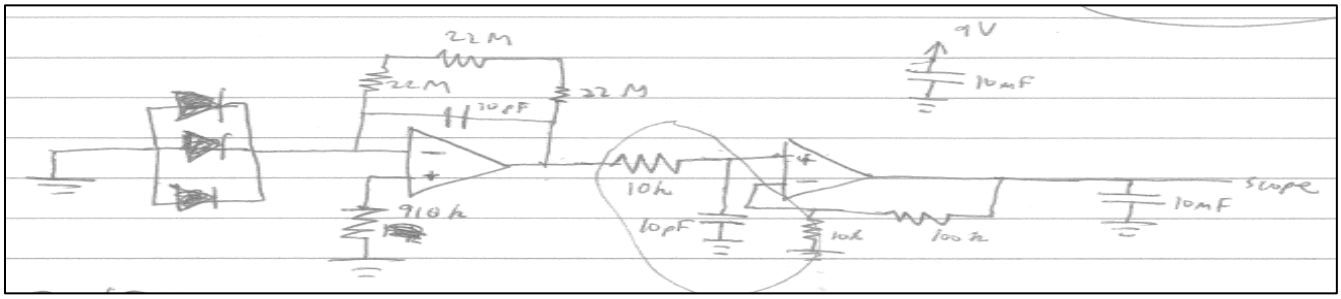

Figure 13 – Hand-Drawn DC Circuit Schematic

A prototype of the DC circuit was placed in the gamma irradiation chamber at BNL. Upon ascertaining that the circuit worked as designed, registering a DC voltage corresponding to

gamma flux as output, a series of output voltage measurements was taken at different distances from the source in the path of the beam. Using the known radiation dose rate at two of the distances, the radiation dose rate at the other distances was estimated with Inverse Square Law. The results of these measurements and estimates are listed in Table 2 and graphed in Figures 14 and 15.

Table 2 – Output Measurements and Estimates for Circuit 5

Distance from Source (in)	Output Voltage (V)	Dose (Rad/hr)
30	8.993	6084
39	4.555	3600 (known)
43	2.35	2961.384532
48	1.69	2376.5625
58	1.25	1627.705113
68	1.046	1184.16955
78	0.956	900 (known)
No Source	0.022	0
No Source (Lights on)	8.995	0

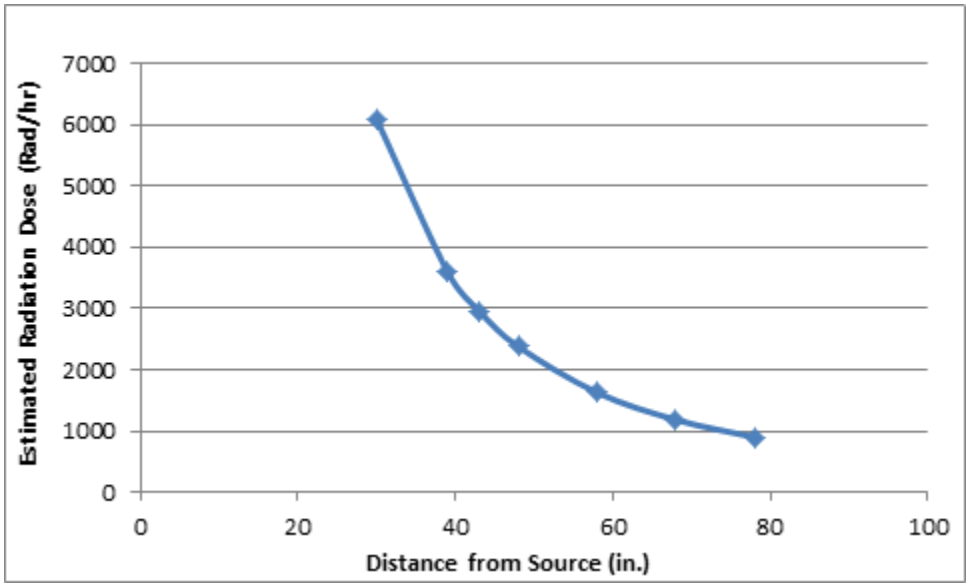

Figure 14 – Estimated Dose Rate versus Distance from Source

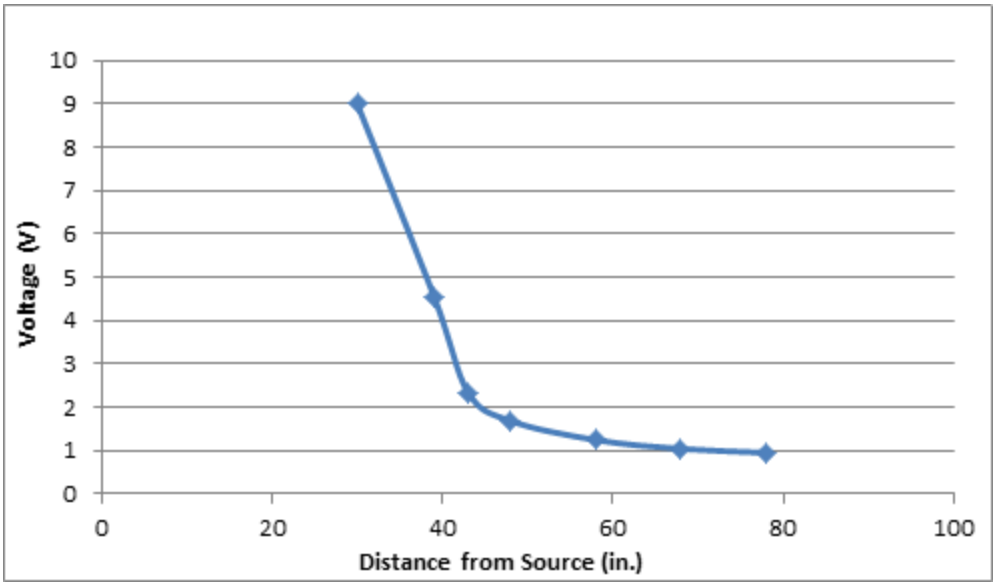

Figure 15 – Output Voltage versus Distance from Source

The correlation between output voltage and distance source resembles the inverse square correlation between dose rate and distance. However, between 40 and 30 inches from the source, the circuit's output voltage increases sharply and saturates. At farther distances the change in voltage is much more flat. One possible reason for the discrepancy is that at distances closer than 40 inches from the source, gamma events are occurring in the PIN diode faster than the circuit's op-amp can process the resulting photocurrents. Utilizing a faster op-amp may result in a correlation bearing greater resemblance to the inverse square.

PCBs were also designed for the DC circuit with DesignSpark PCB; the schematic is shown in Figure 16 and a 3D rendering depicted in Figure 17. The DC PCB is 1.5 inches long and 1 inch wide.

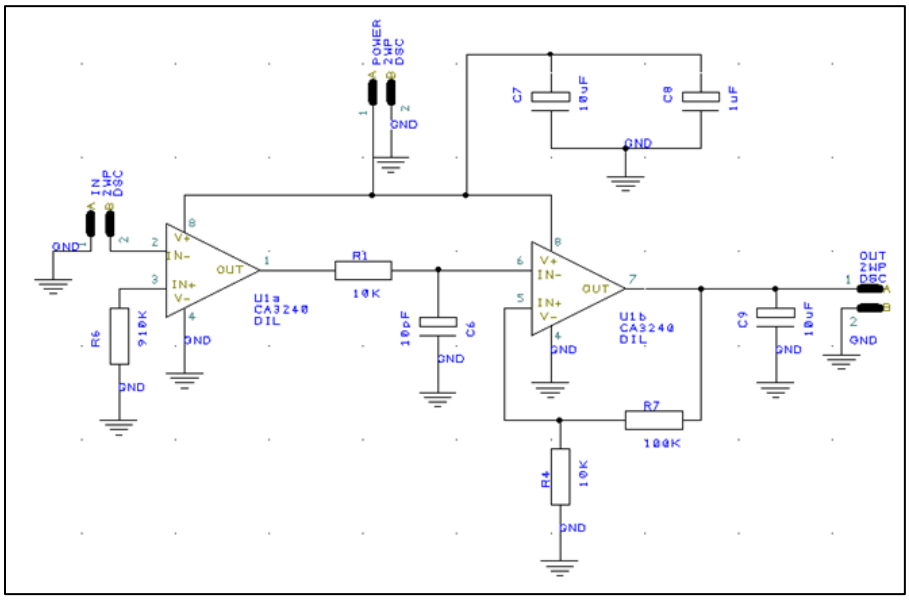

Figure 16 – DC PCB Schematic

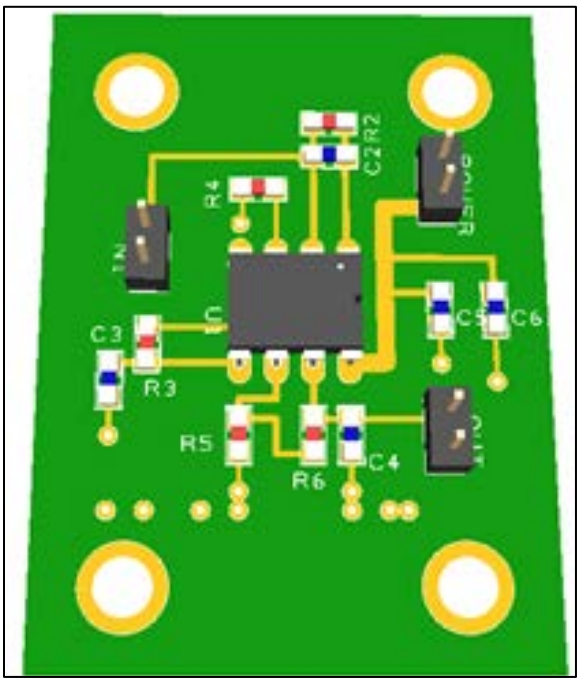

Figure 17 – DC PCB Rendering

After the tests at BNL were completed, a DC PCB was subjected to systematic irradiation tests in the SMU Physics Department's X-RAD iR-160. The PCB was kept outside the x-ray chamber, while a photodiode probe was inserted through the cable passage into the chamber. The probe consisted of PIN diodes wrapped in alternating layers of aluminum foil and black electrical tape to block visible light and electronic background noise. The x-ray voltage was first left constant and then the current was increased by 0.5 mA increments until either the output saturated or until the highest possible current for the given voltage was reached. At each point, the DC level output voltage of the circuit was measured with a digital oscilloscope and recorded. X-ray voltage started at 7.5 kV and was then increased by 7.5 kV increments until the maximum of 160 kV was reached. For x-ray voltages of less than 30 kV, output voltage did not increase appreciably.

Figure 18 displays selected results of this constant voltage experiment, while Figure 19 graphs all such results. Output voltage increases linearly with x-ray current until saturation. The slope and initial output (for a 0.5 mA x-ray current) both depend on the x-ray voltage; a higher x-ray voltage results in a higher output voltage slope and initial output. Some data series, such as that for an x-ray voltage of 45 kV, exhibits slight variations away from a linear correlation. This can be attributed to error associated with the method of data acquisition. Even though the output was a DC voltage, the circuit's output varied slightly with time due to electronic background and variations in the x-ray emissions within the iR-160. When collecting the data, the output voltage was not recorded instantaneously but rather after several seconds. Also, the output became very noisy right before saturation, with a sawtooth waveform of amplitude on the order of 0.1-1 V visible.

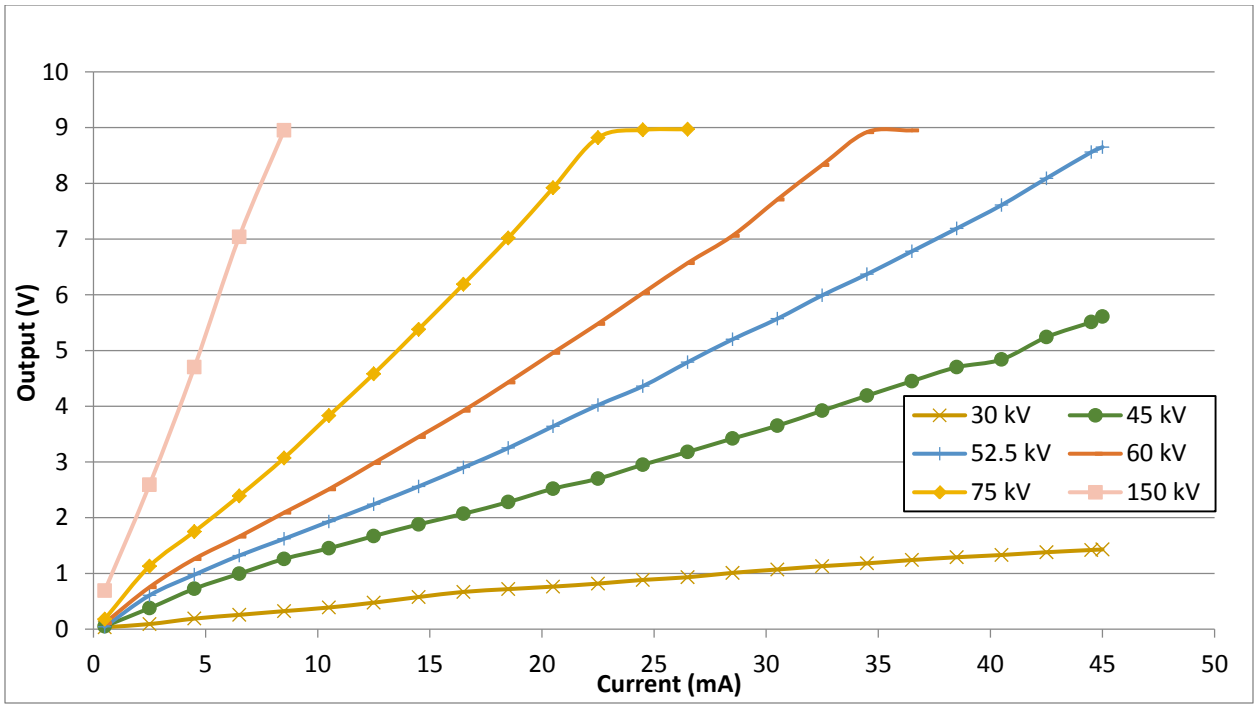

Figure 18 – Selected Constant X-Ray Voltage Calibration Data

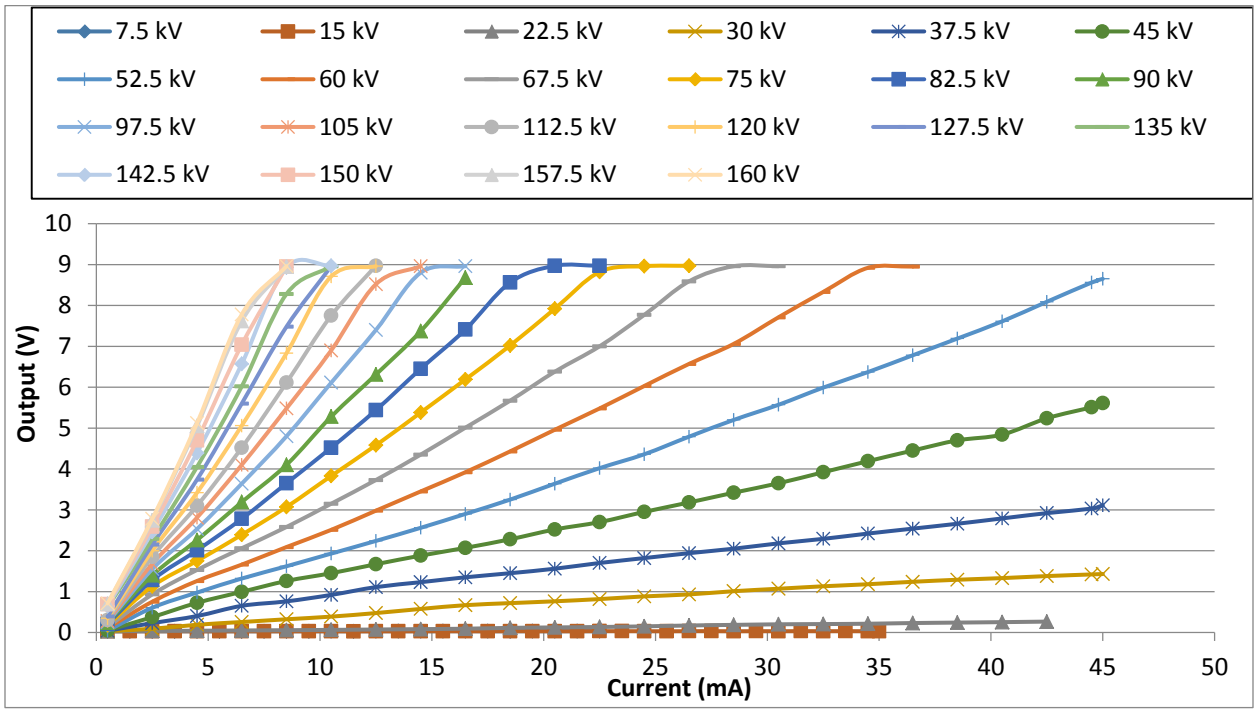

Figure 19 – All Constant X-Ray Voltage Calibration Data

Figure 20 graphs the output voltage for a constant 8.5 mA x-ray current and variable x-ray voltage, utilizing the same data as Figures 18 and 19. Just as with constant x-ray voltage, the output increases roughly linearly until saturation. Additional graphs were not created due to the fact that 8.5 mA is the highest x-ray current that x-ray voltages higher than 142.5 kV could reach

before the circuit saturated. However, based on the results for constant voltage, it can be assumed that output increases linearly for all other currents at a rate proportional to the x-ray current.

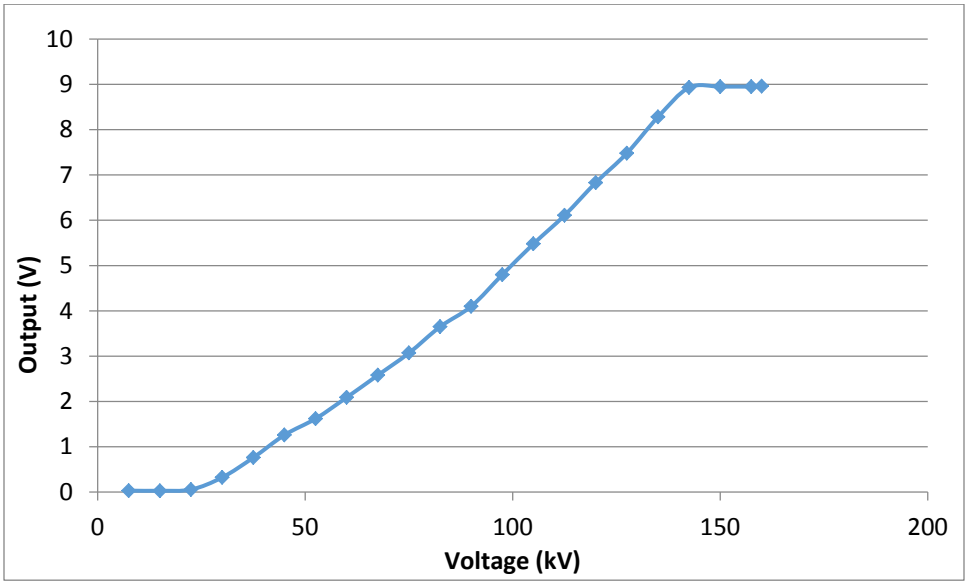

Figure 20 – Constant X-Ray Current Calibration Data, $I_{x\text{-}ray}$=8.5 mA

All of the x-ray calibration was conducted with a photodiode probe placed 70 cm directly below the x-ray source. Figures 21 displays the output voltage for constant x-ray voltage of 105 kV, constant x-ray current of 8.5 mA, and variable distances from the source separated by 10 cm increments. Figure 22 displays the output voltage for variable distances from the source, constant 160 kV x-ray voltage, and constant 1 mA x-ray current. However, the output at each distance varied with each reading. In Figure 22, the output decreased in proportion with the reciprocal of distance squared, as theory dictates for any point radiation source. For the trial in Figure 21, though, the decrease in output voltage was much more irregular. The reasons for this are unclear, but the most likely causes were electronic background noise or radiation damage to the photodiode probe or cable within the x-ray machine.

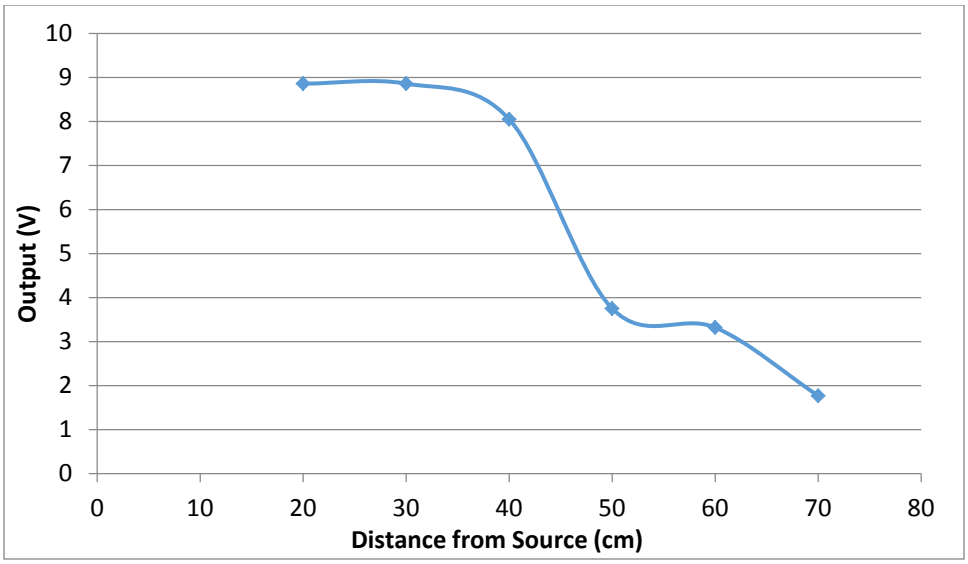

Figure 21 – Output Voltage versus Distance from Source, $V_{x\text{-}ray}$=105 kV, $I_{x\text{-}ray}$=8.5 mA

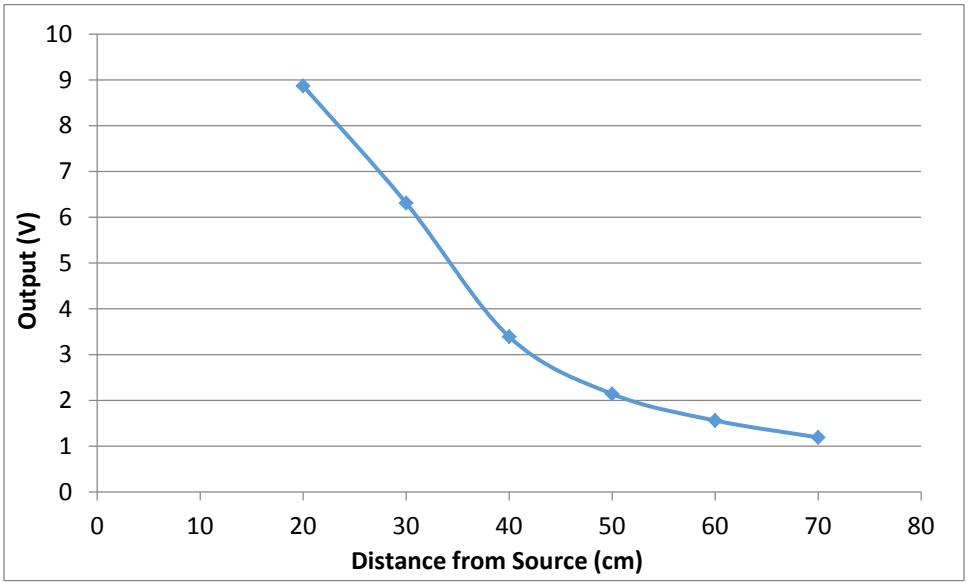

Figure 22 – Output Voltage versus Distance from Source, $V_{x\text{-}ray}$=160 kV, $I_{x\text{-}ray}$=1 mA

V. Readout System

The current stage of this project, as of the submission of this report in April 2014, is to design and implement a readout system to combine the AC and DC circuits. The AC circuit is to be used as a pulse counter at lower dose rates, and the DC circuit is to be used at higher dose rates. Two parallel approaches are being pursued. One is to interface an oscilloscope with a laptop via a USB cable and software downloaded from the oscilloscope's manufacturer. The other is to connect the circuits to a ST Microelectronics STM32F051R8T6 microcontroller. Currently, the Cremat CSP and GSA are being used to process the input from the PIN diodes; the AC and DC circuits will be used once the microcontroller is ready.

As of the submission of this report, the Cremat amplifiers and laptop-oscilloscope interface have been used to characterize β events as a proof of concept. Figure 23 depicts a β event observed by the oscilloscope, as well as the interface provided by the OWON Oscilloscope Software for the OWON SDS7072V oscilloscope. The interface allowed for easy measurement of the pulse height and estimation of the charge and energy deposited using the procedure described in Section II. However, the estimation of frequency was somewhat crude; the oscilloscope was set to single acquisition mode, and the number of pulses triggered over the course of a minute was counted. The average β pulse was 1.6 V in amplitude, resulting in an estimated 127 fC and 0.874 MeV deposited at a frequency of 1.83 Hz. The charge and energy estimates are twice as high as those made previously; the source of this discrepancy has yet to be identified.

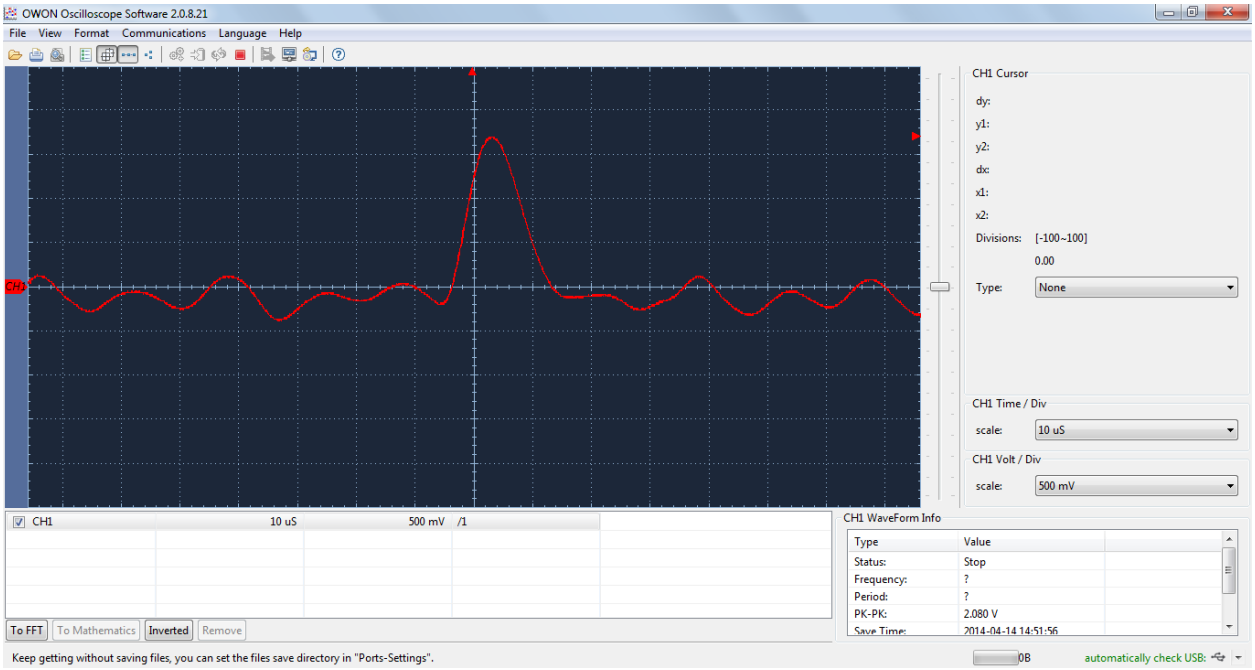

Figure 23 – β Pulse and Laptop-Oscilloscope Interface

VI. Future Work

Once the error in the estimation of charge and energy deposited for β events is corrected, the procedure will be repeated for γ and cosmic μ events with the laptop-oscilloscope interface. When the microcontroller is ready, it will be connected to the Cremat amplifiers and used to characterize β, γ, and μ to determine reliability. The microcontroller will then be interfaced with the AC and DC circuits, and the β, γ, and μ will be characterized once again to verify the combined system's reliability. After that, the AC-DC-microcontroller system will be used to estimate the dose rate and x-ray flux of the X-Rad iR-160. Further work with this project will be to refine the system and construct a sampling electromagnetic calorimeter to measure electrons, gamma photons, and x-rays.

VII. References

1. *Determination of X-Ray Flux Using Silicon Pin Diodes.* **Owen, Robin L., et al., et al.** 2, 2009, Journal of Synchrotron Radiation, Vol. 16, pp. 143-151.

2. **Beatty., J. J., et al., et al.** *Cosmic Rays.* [PDF] s.l. : Lawrence Berkeley National Laboratory, February 16, 2012.

3. Radiation-Watch.org. *Radiation-Watch.org.* [Online] 2011. [Cited: April 14, 2014.] http://www.radiation-watch.org/p/english.html.